Heliyon 10 (2024) e28082

Contents lists available at ScienceDirect

Heliyon

journal homepage: www.cell.com/heliyon

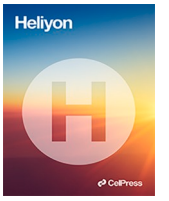

Research article

Functional investigation of a novel *ANKRD11* frameshift variant identified in a Chinese family with KBG syndrome

Shuoshuo Wei [a,b], Yanying Li [a,c], Wanling Yang [d], Shuxiong Chen [a,b], Fupeng Liu [a,b], Mei Zhang [a,c,**], Bo Ban [a,b,c,***], Dongye He [a,b,*]

[a] *Department of Endocrinology, Genetics and Metabolism, Affiliated Hospital of Jining Medical University, Jining, PR China*
[b] *Medical Research Center, Affiliated Hospital of Jining Medical University, Jining, PR China*
[c] *Chinese Research Center for Behavior Medicine in Growth and Development, Jining, PR China*
[d] *Department of Paediatrics and Adolescent Medicine, The University of Hong Kong, PR China*

A R T I C L E I N F O

Keywords:
KBG syndrome
ANKRD11 gene
Whole-exome sequencing
Frameshift variant
Truncated transcript
Functional assays

A B S T R A C T

KBG syndrome is a rare autosomal dominant condition characterized by multisystem developmental disorder, primarily caused by loss-of-function variants in ankyrin repeat domain-containing protein 11 (ANKRD11). Approximately 80 % of *ANKRD11* variants associated with KBG syndrome, are frameshift and nonsense variants. Current insight into the pathogenesis of KBG syndrome resulting from *ANKRD11* truncating variants remains limited. Here, we presented two members from a non-consanguineous Chinese pedigree both exhibiting characteristics fitting the KBG syndrome-associated phenotypic spectrum. Whole-exome sequencing identified a novel heterozygous frameshift variant in ANKRD11 (NM_013275.6, c.2280_2281delGT, p.Y761Qfs*20) in the proband. Sanger sequencing confirmed that the variant was inherited from her mother and co-segregated with KBG syndrome phenotype. *In vitro* functional assays revealed that the frameshift variant escaped nonsense-mediated mRNA decay, and resulting in a truncated protein with significantly increased expression levels compared to full-length ANKRD11. Immunofluorescence results demonstrated that truncated protein was predominantly expressed in the nucleus of HEK293 cells, while wild-type ANKRD11 was equally distributed in both the nucleus and cytoplasm. Moreover, the truncated protein significantly reduced *CDKN1A/P21*-promoter luciferase activity in comparison to wild-type ANKRD11 protein, as well as a remarkably decrease in the endogenous *CDKN1A/P2*1 mRNA level in HEK293 cells. These findings suggest a loss of transcriptional activation function and potentially a dominant-negative mechanism. Overall, our study expands the mutational spectrum of *ANKRD11* gene and provides new insights into the pathogenic mechanism of KBG syndrome caused by *ANKRD11* truncating variants.

* Corresponding author. Department of Endocrinology, Genetics and Metabolism, Affiliated Hospital of Jining Medical University, Jining, PR China.

** Corresponding author. Department of Endocrinology, Genetics and Metabolism, Affiliated Hospital of Jining Medical University, Jining, PR China.

*** Corresponding author. Department of Endocrinology, Genetics and Metabolism, Affiliated Hospital of Jining Medical University, Jining, PR China.

E-mail addresses: zhangmeijn@163.com (M. Zhang), banbo2011@163.com (B. Ban), hehe0917@mail.jnmc.edu.cn (D. He).

https://doi.org/10.1016/j.heliyon.2024.e28082
Received 30 October 2023; Received in revised form 11 March 2024; Accepted 12 March 2024
Available online 13 March 2024

1. Introduction

First described by Herrmann et al., in 1975 and named after the surnames (K–B-G) of three non-consanguineous families with similar phenotype, KBG syndrome (OMIM#148050) is typically characterized by intellectual diability, macrodontia of the upper central incisors, distinctive craniofacial malformations, short stature and multiple skeletal anomalies [1,2]. The molecular etiology of KBG syndrome was not discovered until 2011 when *ANKRD11* mutations were identified through the application of next-generation high-throughput DNA sequencing technology in clinical and molecular genetic studies [3]. Currently, ClinVar database has recorded more than 450 pathogenic or likely pathogenic *ANKRD11* variants, predominantly frameshift and nonsense variants, suggesting that the number of KBG syndrome patients far exceeds the previously reported 340 cases [4]. Statistically, among the 253 KBG syndrome patients harbouring *ANKRD11* variants, 100 %, 80 %, 77 %, 52 %, 38 % and 29 % exhibited craniofacial anomalies, macrodontia of the upper central incisors, intellectual diability, short stature, hearing loss, and congenital heart defect, respectively [5].

ANKRD11 gene, located on chromosome 16q24.3, encodes an ankyrin repeat domain-containing protein that is relatively conserved across species and ubiquitously expressed in various organs and tissues. ANKRD11 plays a crucial role in proliferation, neurogenesis and neuronal localization of cortical neural precursor cells via regulating the acetylation of H3K9, H4K5, H4K8 and H4K16 on downstream target genes [6]. Moreover, ANKRD11 is involved in the regulation of pyramidal neuron migration and dendritic differentiation of mouse cerebral cortex via coordinating with P/CAF to acetylate p53 and H3, subsequently activating brain-derived neurotrophic factor (BDNF)/tyrosine receptor kinase B (TrkB) signaling pathway [7]. Additionally, in heterozygous neural crest-specific ANKRD11-mutant mice, multiple ossification centers in the middle facial bone failed to expand or close. These mice exhibited delayed bone maturity and severely limited bone remodeling [8]. Recent research demonstrated that conditional knockout of ANKRD11 in murine embryonic neural crest caused severe congenital cardiac defect, and the underlying mechanism involved decreased semaphorin3C (Sema3C) expression, as well as reduced mammalian Target of Rapamycin (mTOR) and bone morphogenetic protein (BMP) signaling within cardiac neural crest cells in the outflow tract [9]. These fundamental studies provide robust evidence linking *ANKRD11* gene defects to a partial KBG syndrome phenotype, which includes intellectual disability, craniofacial anomalies and congenital heart defect. Despite ANKRD11 haploinsufficiency being recognized as the inherited molecular etiology of KBG syndrome, the impact of disease-causing variants on ANKRD11 expression or function is still poorly understood, irrespective of whether they are missense variants or truncating variants.

In this study, we identified a novel heterozygous frameshift variant in the *ANKRD11* gene in a Chinese girl with KBG syndrome, which inherited from her affected mother. To improve our understanding of KBG syndrome pathogenesis resulting from *ANKRD11* truncating variants, we performed in-depth investigations into the impact of the frameshift variant on ANKRD11 expression, intracellular localization and transcriptional regulation function using *in vitro* functional approaches.

2. Materials and methods

2.1. Patients and ethical approval

The proband and other family members were recruited from Department of Endocrinology, Genetics and Metabolism at the Affiliated Hospital of Jining Medical University. This study was approved by the Ethics Committee of Affiliated Hospital of Jining Medical University (2021C124, Jining, Shandong, China) in accordance with the principles outlined in the Declaration of Helsinki. All participants and/or their legal guardian signed informed consent prior to the study.

2.2. Clinical evaluation

The proband' clinical parameters were obtained by retrospective review of medical records: gender, birth length, birth weight, gestation, chronological age, bone age, height, body weight, body mass index (BMI), growth hormone (GH) peak, insulin-like growth factor 1 (IGF-1), insulin-like growth factor binding protein 3 (IGFBP-3), chromosomal karyotype and family history. Additionally, a comprehensive assessment of phenotypic features was conducted, including facial characteristic, hearing status, intellectual ability, dental, skeletal and cardiac development. Bone age was assessed by X-ray images of the left hand. Serum levels of GH peak, IGF-1, and IGFBP-3, as well as height standard deviation score (SDS), weight SDS and BMI SDS, were either measured or calculated following established protocols [10]. Hearing status was evaluated through pure tone audiometry and impedance audiometry. Skeletal development, including hand, feet, and spine, were evaluated by X-ray examinations. Cardiac structure and function were analyzed using colorDoppler echocardiography. Intelligence quotient (IQ) was independently evaluated by a physician at the child health clinic using Wechsler Intelligence Scale for Children-Revised (WISC-R) test [11].

2.3. Genomic DNA extraction and whole-exome sequencing

Two milliliters of peripheral blood were collected from the proband and other family members, and genomic DNA samples were extracted using the Blood DNA Midi Kit (D3494-04, Omega Bio-Tek, GA, USA). 1 μg of DNA sample was subjected to shearing into fragments, followed by whole exome capture with the Agilent SureSelect V6 capture kit (Agilent Technologies, CA, USA). The captured DNA was then sequenced on the BGISEQ-500 platform (BGI, Shenzhen, China) with 150 bp pair-end reads and a mean coverage of 130 x across the targeted regions. Valid sequencing data were aligned to the reference human genome (GRCh37/hg19) using Burrows-Wheeler Aligner software (BWA) (version 0.7.15). WES data processing and candidate variant analysis were performed as

previously described [10]. Pathogenic variant was screened following the guidelines of the American College of Medical Genetics and Genomics and the Association for Molecular Pathology (ACMG/AMP), and visualized using Integrative Genomics Viewer (IGV) (version 2.8.10). Additionally, the R package ExomeDepth was applied to detect copy number variation (CNV). DNA samples from the proband and other family members were further applied to validate pathogenic variants through Sanger sequencing.

2.4. Sanger sequencing

The full-length *ANKRD11* coding sequence (NM_013275.6) was downloaded from the NCBI database. Polymerase chain reaction (PCR) primer was designed using Primer Premier 5 software (Eurogentec, USA) and synthesized by Sangon Biotech co., Ltd. (Shanghai, China). 2 × Taq PCR Mix was used for PCR amplification. Primer sequences were as follows: up-stream primer 5′-GCA-GAATCTTCCCTATAAACC-3'; downstream primer 5′-GTCAGATAAGGCTATACTGTTAGA-3'. PCR amplification was performed with an initial denaturation step at 95 °C for 5 min, followed by 10 cycles at 94 °C for 30 s, 63 °C for 30 s and 72 °C for 30 s, and then 30 cycles at 95 °C for 30 s, 58 °C for 30 s and 72 °C for 30 s, and a final extension step at 72 °C for 10 min. The purified PCR product was sequenced on an ABI 3730XL sequencer (Foster City, USA).

2.5. Plasmids construction

Wild-type (WT) human *ANKRD11* and mutant *ANKRD11* complementary DNA (cDNA) sequences were synthesized and subsequently inserted into an eukaryotic expression vector (GV657, GeneChem, Shanghai, China). 3 x Flag tag was fused to the C-terminus of both WT *ANKRD11* and mutant *ANKRD11* sequences. An empty vector lacking *ANKRD11* sequence was used as a negative control. The integrity of *ANKRD11* sequence within the plasmid constructs was confirmed via Sanger sequencing.

2.6. Cell culture and transfection

Human embryonic kidney (HEK293) cells were obtained from the Cell Bank at the Chinese Academy of Sciences (Shanghai, China), and were cultured in Dulbecco's Modified Eagle Medium (Gibco), supplemented with 10 % heat-inactivated fetal bovine serum (Gibco) and 100 U/mL penicillin-streptomycin (Gibco) at 37 °C in a humidified atmosphere containing 5 % CO_2 and 95 % air. HEK293 cells were seeded in 6-well plates, and when the cells reached 50–60 % confluence, 2.5 μg of plasmids per well were transfected using Lipofectamine™ 3000 (Thermo Fisher Scientific, MA, USA) following the manufacturer's standard instructions. Approximately 48 h after transfection, cells were harvested and used for subsequent experiments, including quantitative real-time polymerase chain reaction (qRT-PCR), western blotting, and immunofluorescence imaging.

2.7. Quantitative real-time polymerase chain reaction (qRT-PCR)

Total RNA sample was isolated using TRIzol reagent (Thermo Fisher Scientific, MA, USA). 1 μg of each RNA sample was reverse transcribed into cDNA using HiScript III RT SuperMix for qPCR (+gDNA wiper) (R323-01, Vazyme, Nanjing, China) following the manufacturer's instructions. qRT-PCR was performed with Taq Pro Universal SYBR qPCR Master Mix (Q712-02, Vazyme, Nanjing, China) in a 20 μL reaction volume on the QuantStudio 5 real-time PCR detection platform (ABI, USA). Melting curves were analyzed to ensure the amplification of a single amplicon. The results were analyzed by the $2^{-\triangle\triangle CT}$ method using *GAPDH* gene for normalization. All primer sequences were listed in Table 1.

2.8. Western blotting

Cells were lysed using RIPA lysis buffer (P0013B, Beyotime, China) supplemented with protease inhibitor (P1045, Beyotime, China), and protein concentration was determined with the BCA protein assay kit (P0010, Beyotime, China). Equal amounts of protein (30 μg) were loaded onto 7.5 % sodium dodecyl sulfate-polyacrylamide gel electrophoresis (SDS-PAGE) and subsequently transferred to a polyvinylidene fluoride (PVDF) membrane (Millipore, USA). The membrane was then blocked with 5 % non-fat milk for 1 h at room temperature and incubated overnight at 4 °C with following primary antibodies at an appropriate dilution ratio: mouse monoclonal anti-Flag antibody (F9291, Sigma, 1:1000) and rabbit polyclonal anti-β-actin antibody (81115-1-RR, Proteintech, 1: 7500). After washing three times with TBS-T buffer, the membrane was incubated with horse radish peroxidase-conjugated (HRP) goat anti-mouse IgG (H + L) antibody (AS003, ABclonal, 1: 5000) and HRP goat anti-rabbit IgG (H + L) antibody (AS041, ABclonal, 1: 5000) for 1 h at room temperature. The membrane was washed again, followed by incubation with SuperFemto ECL Chemiluminescence Kit (E423, Vazyme, China), and the signals were visualized using Tanon 5800 Imaging System (Shanghai, China).

Table 1
Primer sequences for amplifying *ANKRD11, CDKN1A/P21* and *GAPDH gene*.

Target gene	Forward primer (5′-3′)	Reverse primer (5′-3′)
ANKRD11	GCAGGGCCCTGAGCGGAAGAGG	CTGGGCTGTTGGCAGACTCCTC
CDKN1A/P21	TCCGTCAGAACCCATGCGGC	CAGGCGAAGTCACCCTCCAGTG
GAPDH	GGAGCGAGATCCCTCCAAAAT	GGCTGTTGTCATACTTCTCATGG

Protein band intensities were further quantitatively analyzed using ImageJ software (NIH, USA).

2.9. Immunofluorescence imaging of intracellular localization

Cells grown on glass coverslips were washed twice with phosphate-buffered saline (PBS) and subsequently fixed with 4% paraformaldehyde for 30 min. Cells were then permeabilized with a 0.5 % Triton X-100 solution (T8200, Solarbio, China) for 20 min, followed by a 1 h blocking step with 5 % bovine serum albumin (BSA) (SW3015, Solarbio, China) at room temperature. The cells were then incubated with Anti-Flag (20543-1-AP, Proteintech, 1: 100) for 2 h at 37 °C, followed by 1 h-incubation with Coralite594-conjugated goat anti-rabbit IgG (H + L) antibody (SA00013-4, Proteintech, 1: 500). Finally, the cells were counterstained with DAPI (P0131, Beyotime, China) to visualize the nuclei. Fluorescence images were captured simultaneously in the red, green, and blue channels using a confocal laser scanning microscope equipped with a 20× objective (LSM800, Carl Zeiss, Germany). For quantitative analysis, nine positively stained cells from different fields of view in each group were selected, and the ratio of cytoplasm to nuclear fluorescence intensity was determined using ZEN software (Zeiss, Germany).

2.10. Dual-luciferase reporter assays

Two firefly luciferase reporters constructs, namely pGL4.10-*CDKN1A/P21* promoter 1-Luc and pGL4.10-*CDKN1A/P21* promoter 2-Luc, were generated by synthesizing two *CDKN1A/P21* promoters and cloning them into a pGL4.10 vector obtained from OBIO Technology (Shanghai, China). Two *CDKN1A/P21* promoter sequences were obtained from pGL2-*p21* promoter-Luc (Addgene_33021) and WWP-Luc (Addgene_16451), respectively, and further confirmed by Sanger sequencing. HEK293 cells were seeded in 6-well plates, and when cells reached 50–60 % confluence, 1 μg of firefly luciferase reporter vector, 20 ng of pRL-CMV Renilla luciferase normalization control together with 2 μg of expression vector containing WT, mutant, or null ANKRD11 were transiently co-transfected using Lipofectamine™ 3000 (Thermo Fisher Scientific, USA) (Fig. 1). After 48 h transfection, firefly luciferase and Renilla luciferase activities were measured using a Renilla-Firefly Luciferase Dual Assay Kit (HY–K1013, MedChemExpress, Germany) following the manufacturer's instructions on a GloMax® 20/20 Luminometer (Promega, USA).

2.11. Statistical analysis

Values were representative of three independent assays and expressed as mean ± SD. Statistical analysis was conducted by Student's *t*-tests or one-way analysis of variance (ANOVA) followed by Dunnett's post hoc test using GraphPad Prism version 8.3.0 (GraphPad Software Inc., San Diego, CA, USA). A significance level of $p < 0.05$ was considered statistically significant among the groups. Significance levels were denoted as follows: $^{*}p < 0.05$, $^{**}p < 0.01$, $^{***}p < 0.001$, or $^{****}p < 0.0001$.

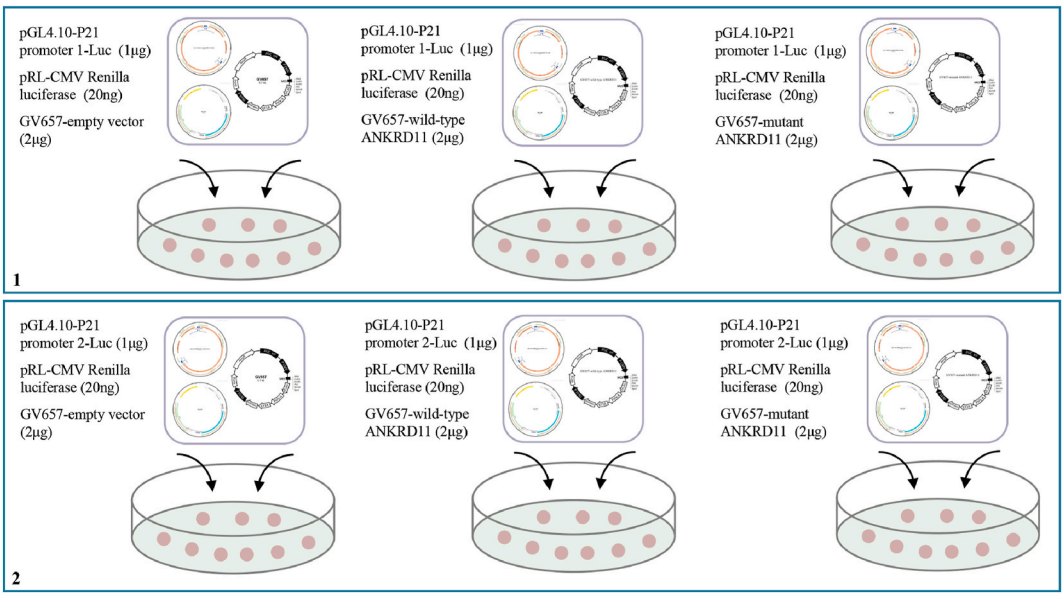

Fig. 1. Schematic representation of dual-luciferase reporter assays. Number 1 represents first reporter assay using *CDKN1A/P21* promoter 1, and number 2 represents second reporter assay using *CDKN1A/P21* promoter 2.

3. Results

3.1. Clinical characteristics

The proband was a Chinese girl who was born small for gestational age at full-term, with a birth weight of 1.0 kg (<3rd centile) and a body length of 42 cm (−4.5 SD). Her mother displayed distinct physical features including thick eyebrows, dental irregularities and wide upper central incisors, high-arch and narrow palate, mild scoliosis, fifth finger brachydactyly, shortened fourth metatarsal bones bilaterally, otitis media and hearing impairment (Fig. 2A). Notably, despite slightly unclear speech, her mother exhibited normal communication abilities. The girl was the first child of non-consanguineous parents and was bottle-fed from birth. At six months old, she was diagnosed as having congenital heart defect, which eventually closed by the age of 5 years without surgical intervention. The proband first sought medical attention at the age of 7 years and 2 months due to growth retardation (height: 107.8 cm, −2.88 SD). At that time, her weight was 13 kg (−2.74 SD) with a BMI of 11.19 kg/m^2 (−3.51 SD). Tests revealed a peak GH value of 14.992 ng/ml by a levodopa GH test, IGF-1 level at 75.75 ng/mL (reference value: 76–499 ng/mL), and IGFBP-3 level at 2.84 μg/mL (reference value: 1.4–6.1 μg/mL). Bone X-ray of the left hand indicated extremely delayed bone age (bone age minus chronological age: 3.17 years) (Fig. 2B). Hearing status remained unaffected. The patient did not receive growth-promoting drug therapy. When the girl was 16 year and 7 months, her height was 141.3 cm (−3.42 SD), weight was 33 kg (−4.36 SD), and BMI was 16.53 kg/m^2 (−1.53 SD). Bone X-ray of the left hand indicated almost complete closure of the epiphyseal plate (Fig. 2C). Alongside severe short stature, she exhibited distinct facial and skeletal anomaliess including thick eyebrows, wide upper central incisors, high-arch narrow palate, short hands, short feet, scoliosis and fifth finger brachydactyly (Fig. 2C). Echocargiography showed protrusion at the membranousportion of the interventricular septum, left ventricular false tendon, and tricuspid regurgitation (Fig. 2D). Additionally, her IQ was independently assessed by a physician at the child health clinic and WISC-R test score was less than 40, indicating an intellectual disability (Fig. 2E).

3.2. Identification of a novel frameshift variant in the ANKRD11 gene

WES analysis identified a novel heterozygous frameshift variant in the *ANKRD11* gene (g.89350669_89350670del) (Fig. 3A). The genomic alteration was predicted to cause a 2-base pair deletion (c.2280_2281delGT) in exon 9 of *ANKRD11* transcript (NM_013275.6), generating a truncated protein product (p.Tyr761Glnfs*20) (Fig. 3B). This variant was classified as "pathogenic" (PVS1+PM2+PM4+PP1) following the ACMG/AMP guideline and has been submitted to the Leiden Open Variation Database (LOVD) (#0000927440) and ClinVar database (SCV004190196). Sanger sequencing further validated that the frameshift variant in the

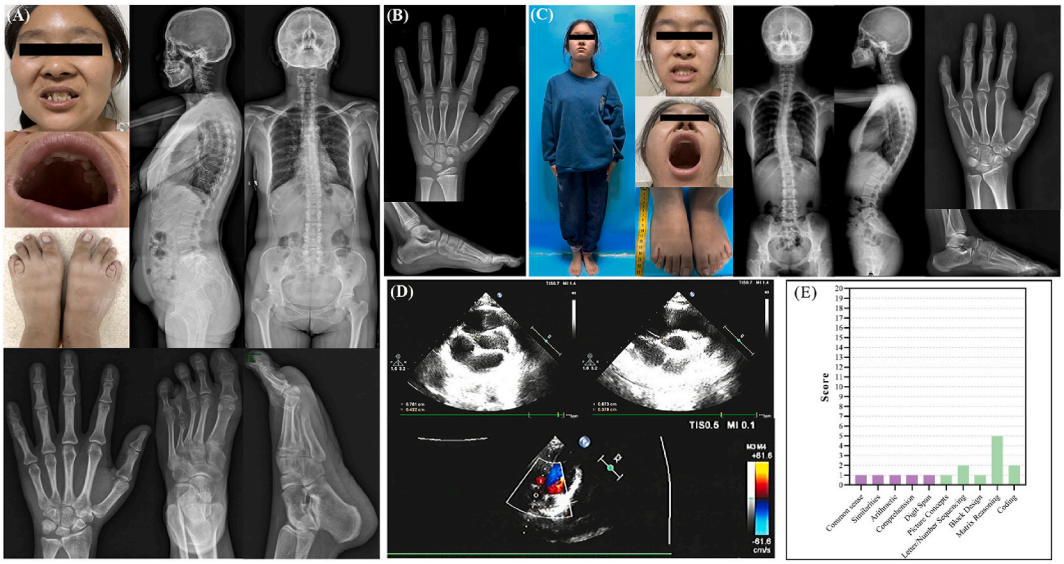

Fig. 2. Clinical features of the proband and her mother with KBG syndrome. (A) Photographs of the proband's mother exhibited thick eyebrows, dental irregularities, wide upper central incisors, high-arch and narrow palate. Bone X-rays showed mild scoliosis, fifth finger brachydactyly and shortened fourth metatarsal bones bilaterally. (B) Bone X-rays of the left hand and left foot showed delayed ossification of the proband at the age of 7 years. (C) Photographs of the proband showed short stature, thick eyebrows, wide upper central incisors, high-arch and narrow palate, and short feet at the age of 16 years. Bone X-rays showed scoliosis and fifth finger brachydactyly, as well as almost completely closed epiphyseal plate. (D) Echocargiography imaging of the proband showed protrusion at the membranousportion of the interventricular septum, left ventricular false tendon and tricuspid regurgitation at the age of 16 years. (E) The scores of each WISC-R subscale for the proband. WISC-R comprises five speech/language subscales (common sense, similarities, arithmetic, comprehension, digit span), highlighted in purple, and five operation subscales (picture concepts, letter/number sequencing, block design, matrix reasoning, coding), highlighted in green. The WISC-R IQ score is the cumulative sum of all subscale scores. It was noted that proband's IQ score was less than 40 at the age of 16 years.

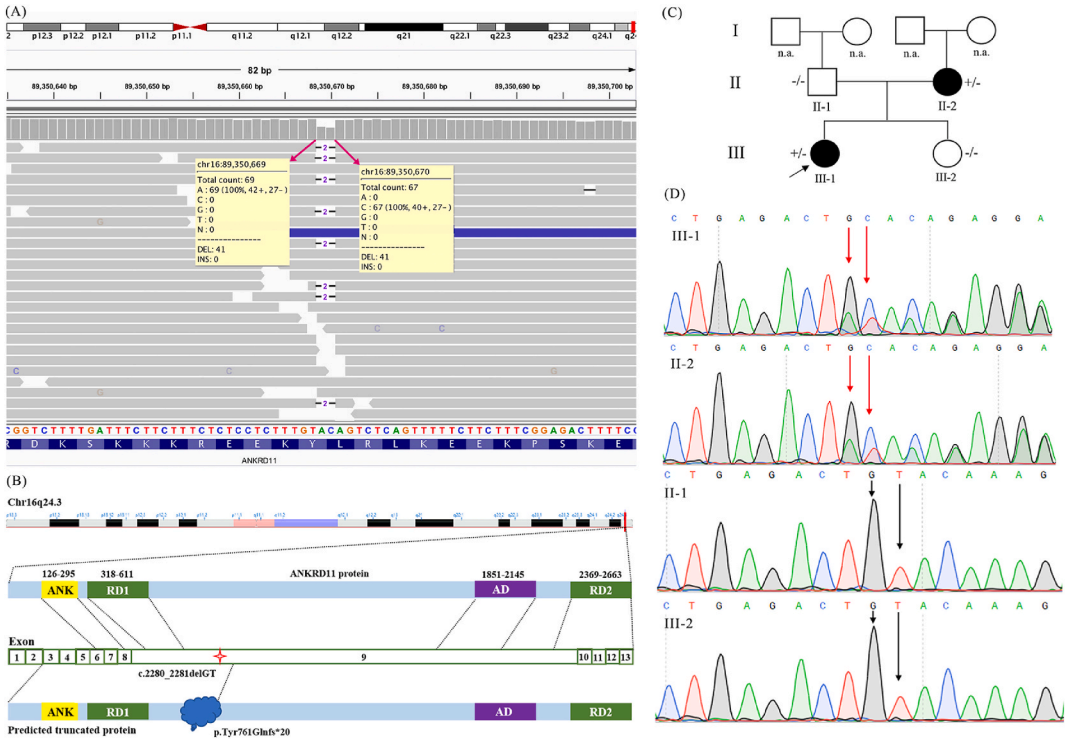

Fig. 3. Molecular findings. (A) 2-base pair deletion (TAC to T) in the *ANKRD11* gene was presented by IGV visualization of WES data. (B) Schematic diagram representing the variation in ANKRD11 transcript (NM_013275.6, c.2280_2281delGT) and encoded protein (p.Tyr761Glnfs*20). (C) Family pedigree of the proband. Square indicates male and circle indicates female. Black and white symbol denote affected and unaffected individuals, respectively. Arrow indicates the proband. n.a.: DNA sample was not available for genetic test. +/−: heterozygous variant is present. −/−: heterozygous variant is not present. (D) Sanger sequencing results of *ANKRD11* variant in the proband and her family members. Red and black arrows indicate the affected and unaffected residues, respectively. A heterozygous *ANKRD11* variant was found in the proband (III-1) and her affected mother (II-2).

proband (III-1) was inherited from her clinically affected mother (II-2) (Fig. 3C&D).

3.3. Effect of frameshift variant on transcription, translation and intracellular localization of ANKRD11

Fluorescence images revealed comparable transfection efficiency between ZsGreen-ANKRD11-WT and ZsGreen-ANKRD11-p.Y761Qfs*20 plasmids in HEK293 cells (Fig. 4A). qRT-PCR results demonstrated a significant increase in the mRNA level of mutant *ANKRD11* compared to WT *ANKRD11* ($p < 0.0001$) (Fig. 4B– Supplementary Table 1). Western blotting analysis indicated that the frameshift variant (p.Y761Qfs*20) encoded a truncated ANKRD11 protein (≈85 kDa), with its expression level notably increased compared to WT ANKRD11 protein (≈292 kDa) ($p < 0.01$) (Fig. 4C). Confocal fluorescent microscopy images revealed that WT ANKRD11 localizated to both the nucleus and cytoplasm, while mutant ANKRD11 was primarily expressed in the nucleus (Fig. 4D). The ratio of cytoplasm to nuclear fluorescence intensity for mutant ANKRD11 was significantly decreased compared to that of WT ANKRD11 ($p < 0.0001$), providing further evidence of the abnormal subcellular localization of mutant protein (Fig. 4D).

3.4. Effect of frameshift variant on transcriptional regulation function of ANKRD11 protein

To determine whether the frameshift variant affect the transcriptional regulation activity of ANKRD11, a dual-luciferase reporter assay was performed using the *CDKN1A/P21* promoter, a well-known downstream target. The results showed that both WT and mutant ANKRD11 significantly increased luciferase activity by activating two *CDKN1A/P21* promoters compared to empty vector control ($p < 0.05$), however, mutant ANKRD11 (p.Y761Qfs*20) showed a more dramatically decrease in luciferase activity compared to WT ANKRD11 ($p < 0.001$) (Fig. 5A&B, Supplementary Table 2). Consequently, the frameshift variant led to a diminished transcriptional activation activity of ANKRD11 on the CDKN1A/P21 gene. Additionally, no significant difference in the mRNA levels of endogenous *CDKN1A/P21* gene was observed between WT and empty vector group ($p > 0.05$). In contrast, mutant ANKRD11 significantly decreased *CDKN1A/P21* mRNA level compared with both empty vector control and WT ANKRD11 ($p < 0.05$), suggesting a dominant-negative effect (Fig. 5C–Supplementary Table 3),

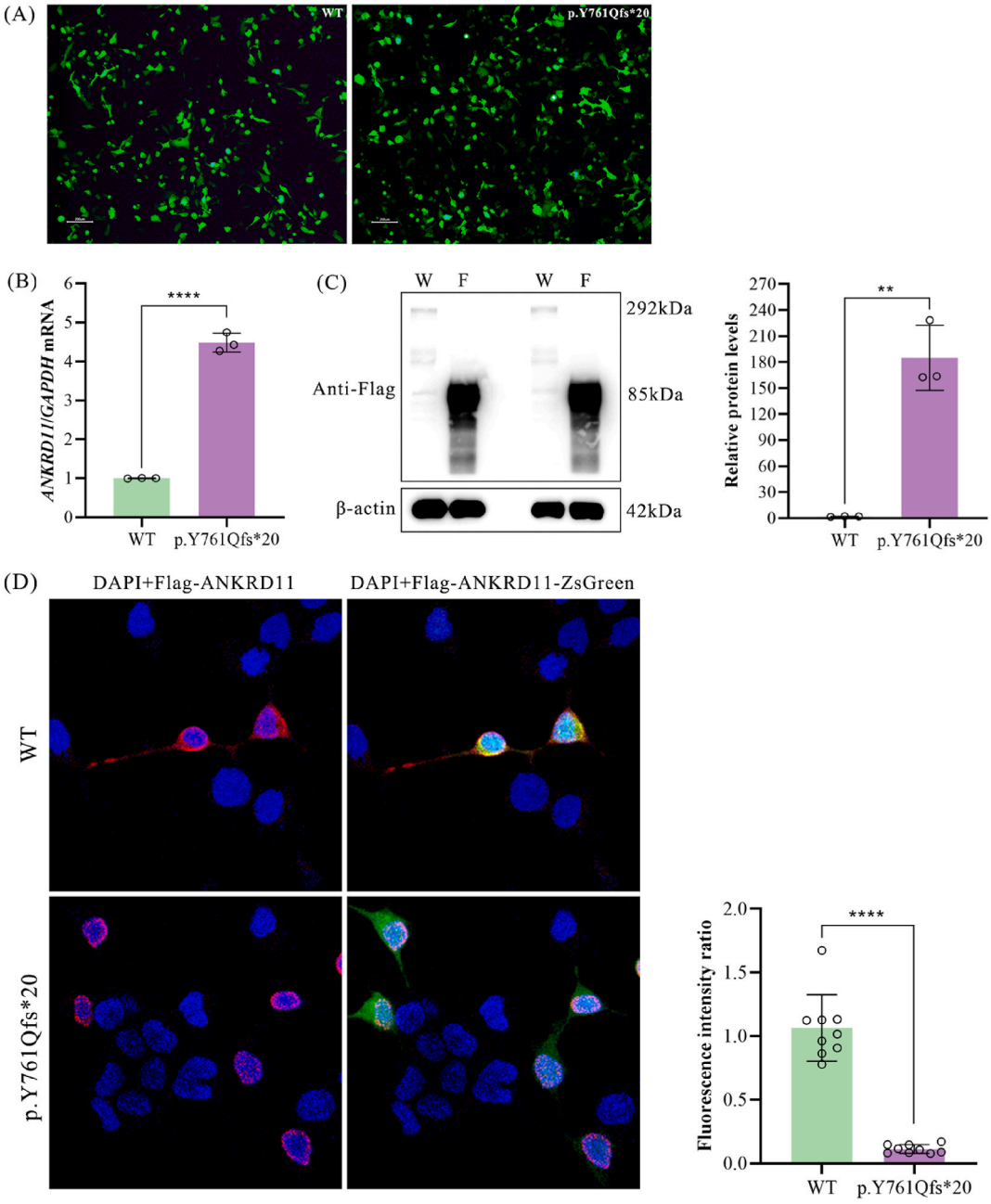

Fig. 4. Effects of frameshift variant in *ANKRD11* (c.2280_2281delGT) on its transcription, translation and intracellular localization in HEK293 cells. (A) Fluorescent images showing transfection efficiency of ZsGreen-ANKRD11-WT and ZsGreen-ANKRD11-p.Y761Qfs*20 plasmids. Scale bar: 200 μm. (B) Relative quantitative analysis of mRNA levels of WT and mutant *ANKRD11* by qRT-PCR. (C) Expression of WT and mutant ANKRD11 protein by Western blot. Two representative protein samples were presented. Uncropped blot is available in Supplementary Fig. 1-ANKRD11 and Supplementary Fig. 2-β-actin. M: Marker. W: wild type. F: frameshift variant. The intensities of protein bands were quantitatively analyzed across three independent experiments. (D) Confocal microscopy images showed the localization of both wild-type (WT) and mutant ANKRD11 proteins labeled with Anti-Flag in red. Nuclei are stained with DAPI (blue), and ZsGreen (green) was used to identify positively transfected cells. The quantitative analysis included determining the ratio of cytoplasmic to nuclear fluorescence intensity for ANKRD11. Values were expressed as the mean ± SD from three independent experiments. Data were analyzed by Student's t-tests. $^{**}p < 0.01$, $^{****}p < 0.0001$.

4. Discussion

In the present study, we presented two members from an non-consanguineous Chinese pedigree both with characteristics fitting the KBG syndrome-associated phenotypic spectrum, and identified a novel heterozygous frameshift variant in *ANKRD11*

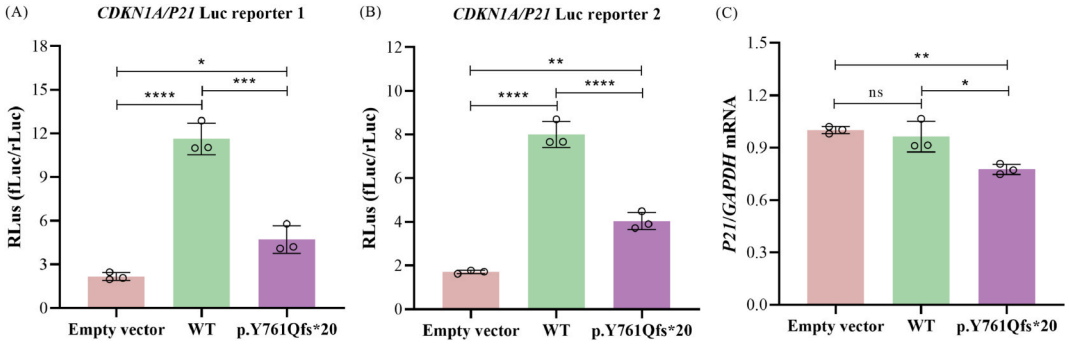

Fig. 5. Effects of frameshift variant in *ANKRD11* (c.2280_2281delGT) on transcriptional activation of downstream *CDKN1A/P21* gene. (A&B) Effects of WT and mutant ANKRD11 protein on activation activity of two *CDKN1A/P21* promoters by dual-luciferase reporter assay. (C) Effects of WT and mutant ANKRD11 protein on mRNA level of endogenous *CDKN1A/P21* in HEK293 cells by qRT-PCR. A ZsGreen-containing construct without *ANKRD11* was used as empty vector control. Values were expressed as the mean ± SD from three independent transfection experiments. Data were analyzed by one-way analysis of variance and a post hoc Dunnett's test. $*p < 0.05$, $**p < 0.01$, $***p < 0.001$, $****p < 0.0001$.

(c.2280_2281delGT, p.Y761Qfs*20) that co-segregated with the phenotype. Our cellular assays revealed that the frameshift variant escaped nonsense-mediated mRNA decay (NMD), leading to the production of a truncated protein. Our investigations further demonstrated that the truncated protein exhibited abnormal intracellular localization, diminished transcriptional regulation function, and potentially exerted a dominant-negative effect (Fig. 6). These novel findings contribute valuable insights into pathogenic mechanism underlying KBG syndrome resulting from *ANKRD11* truncating variant.

KBG syndrome remains underdiagnosed and its precise prevalence is yet to be established, although it recently gained more attention and definitely amongst the most common intellectual disability syndrome recognized by clinicians or clinical geneticists. The expert consensus statement has not been developed for clinical diagnosis of KBG syndrome primarily stems from its broad phenotypic spectrum and significant variations in symptoms among affected individuals, even within the same family or among unrelated individuals with the same *ANKRD11* variant [12–14]. This variability was exemplified in our study by comparing a proband and her affected mother both harbouring a novel frameshift variant in ANKRD11 (p.Y761Qfs*20). They both exhibited thick eyebrows, wide upper central incisors, a high-arch and narrow palate, scoliosis, and fifth finger brachydactyly, whereas the proband manifested severe intellectual disability, short stature, congenital heart defect, short hand and short feet, with no dental irregularities, shortened fourth metatarsal bones bilaterally, unclear speech, otitis media, and hearing impairment observed in her mother. Clinical phenotypic

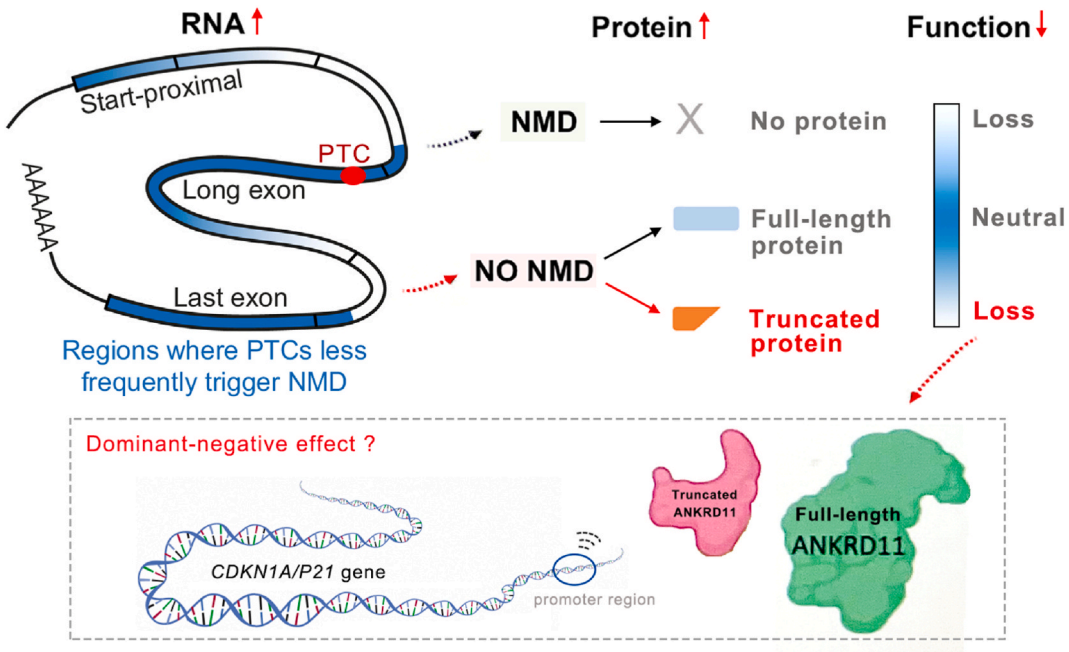

Fig. 6. Schematic diagram of the impact of *ANKRD11* truncating variant (c.2280_2281delGT) on expression and function of encoded protein as shown in red. The truncated protein (p.Tyr761Glnfs*20) might produce a dominant-negative effect that requires more in-depth investigations.

variability is a common characteristic in many rare genetic disorders, even within the same kindred [15]. The incomplete penetrance and variable expressivity of disease-causing variant are associated with common genetic variants, variants in regulatory regions, epigenetics, environmental factors, genetic compensation, and lifestyle choices. These factors explain why apparently unaffected parents can transmit pathogenic variants to affected offspring or why affected parents and offsprings may exhibit different phenotypes [16]. Addtionally, due to technical limitations in WES, there may be undetected gene variations or CNVs in the genome contributing to varying degrees of disease severity. Based on current clinical evidences from case series and literature reviews, macrodontia of the upper central incisors and intellectual disability are the two most frequently observed phenotype, providing crucial diagnostic information for clinicians suspecting KBG syndrome [17–19]. However, despite the absence of obvious intellectual disability in the proband's mother, further investigation through brain magnetic resonance imaging (MRI) is warranted during medical follow-up. Global skeletal abnormalities, esespecially craniofacial anomalies, fifth finger clinodactyly and brachydactyly, are common in KBG syndrom [20–22]. A prior study in mice with heterozygous deletion of *Ankrd11* in neural crest cells or N-ethyl-N-nitrosourea-induced *Ankrd11* heterozygous mutation exhibited craniofacial abnormalities, spinal kyphosis, reduced body length, and an osteopenia-like phenotype, emphasizing the critical role of *ANKRD11* gene in skeletogenesis [8,23]. Both the proband and her mother exhibited high-arch and narrow palate, fifth finger brachydactyly, and scoliosis with varying degree of severity. The affected mother also presented with bilaterally shortened fourth metatarsal bone, resembling a previously reported KBG syndrome case with brachydactyly type E [24]. Moreover, the proband displayed cardiac defects although this occurred in less than 35 % of KBG syndrome patients [25]. While loss-of-function variants in *ANKRD11* leading to intellectual disability, craniofacial anomalies and congenital heart defect have been elucidated well [7–9], further investigations is needed to uncover genotype-phenotype correlations and the mechanisms underlying other phenotypes associated with KBG syndrome.

In addition to clinically recognizable phenotype mentioned above, next generation sequencing (NGS)-based identification of *ANKRD11* pathogenic variants has proven to be an efficient strategy for aiding clinicians in accurately diagnosing KBG syndrome. We identified a novel *ANKRD11* heterozygous frameshift variant (NM_013275.6, c.2280_2281delGT, p.Y761Qfs*20) in a Chinese girl and her mother, both affected by KBG syndrome, using WES technology. To enhance our understanding of how this framshift variant affects the gene/protein, several *in vitro* functional assays were performed. Our findings revealed that the frameshift variant generated a truncated protein with a significantly higher expression level via escaping NMD mechanisms. NMD is an intracellular RNA quality surveillance mechanism capable of degrading aberrant transcripts containing premature termination codons (PTCs) [26]. Notably, statistical analyses of matched genome and transcriptome data indicated that PTCs located in the start-proximal, last exon, last ~50 nt of the penultimate exon and extremely long exons (>400 nt) trigger NMD less efficiently [27]. The frameshift mutation-induced PTC (c.2280_2281delGT) happened to be located in the longest exon 9 of the *ANKRD11* transcript (NM_013275.6), thus initiating NMD evasion and producing a truncated protein with a higher expression level compared to WT protein. Furthermore, we observed that exogenously expressed WT ANKRD11 localized to the nucleus and cytoplasm, whereas truncated protein (p.Y761Qfs*20) predominantly accumulated within the nucleus of HEK293 cells. Despite being a transcriptional co-regulator, the truncated protein did not loss its nuclear import capacity, attributed to the intact N-terminus with a highly conserved 35-amino acid sequence mediating its interaction with Importin α1 [28,29]. Further exploration is required to determine whether certain sequences after the truncation site affect the cytoplasmic localization of ANKRD11 protein. Most importantly, WT ANKRD11 significantly activated the *CDKN1A/p21*-promoter luciferase, consistent with previous report [30]. However, truncated protein exhibited an obvious decrease in transcriptional activation activity compared to full-length ANKRD11. Intriguingly, it significantly down-regulated the mRNA level of endogenous *CDKN1A/P21* gene in HEK293 cells compared to either WT ANKRD11 or empty vector control, suggesting that the truncated protein might exert a dominant-negative effect. Previous report speculated that the pathogenicity of an *ANKRD11* heterozygous variant may imply a dominant-negative mechanism via the formation of a an N-terminus-mediated dimer with WT ANKRD11 [31]. However, whether truncated ANKRD11 protein produces a dominant-negative effect requires more sufficient evidences.

Previous studies have demonstrated that pathogenic *ANKRD11* missense variants or three-base pair deletions resulting in a single-amino-acid deletion did not significantly impact the expression levels of mRNA and protein, as well as nuclear localization, but impair the stability or transcriptional activity of encoded protein, particularly missense variants clustered in the C-terminal repression domain 2 (RD2) [28,30]. In contrast, deletion of first noncoding exon obviously decreased the mRNA level of *ANKRD11* [32]. Taken together, *ANKRD11* frameshift variant (c.2280_2281delGT) appeared to trigger more substantial damage to the gene/protein compared to other variant types. Our observations revealed a higher frequency of developmental delay and intellectual disability, core phenotypes of KBG syndrome, in individuals with truncating variants compared to those with missense variants [33]. Notably, the majority of *ANKRD11* variants that underlie KBG syndrome are frameshift or nonsense variant, predicting a more recognizable phenotype. Overall, This study represents the first investigation into the impact of frameshift variant on the gene expression, intracellular localization and transcriptional regulation function of ANKRD11. To gain a deeper understanding of KBG syndrome pathogenesis, further studies should be performed using clinical samples and model animals to uncover pathogenic mechansim associated with ANKRD11 frameshift variants.

In conclusion, our study identified a novel frameshift variant in the *ANKRD11* gene in a Chinese KBG girl and her affected mother. The frameshift variant resulted in a truncated protein with increased expression level, abnormal intracellular localization and diminished transcriptional activation function. These findings not only expanded mutational spectrum of *ANKRD11* gene, but also offer new perspectives on the pathogenesis of KBG syndrome induced by a heterozygous *ANKRD11* truncating variant.

Funding

This work was supported by the National Clinical Key Specialty Construction Project of China (nfmk2023), and was partly supported by the PhD Research Foundation of Affiliated Hospital of Jining Medical University, China (2018-BS-007).

5. Data availability statement

The *ANKRD11* variant has been submitted to the Leiden Open Variation Database (#0000927440) and ClinVar database (VCV002674640.1). The raw data from qRT-PCR and dual-luciferase reporter assays have been included in the supplementary material. Other data generated during and/or analyzed during the current study are available from the corresponding author upon reasonable request.

Ethical approval

This study was approved by the Ethics Committee of Affiliated Hospital of Jining Medical University (2021C124, Jining, Shandong, China) in accordance with the principles outlined in the Declaration of Helsinki.

CRediT authorship contribution statement

Shuoshuo Wei: Validation, Investigation, Formal analysis, Data curation. **Yanying Li:** Resources, Investigation, Data curation. **Wanling Yang:** Methodology, Conceptualization. **Shuxiong Chen:** Software, Methodology. **Fupeng Liu:** Resources. **Mei Zhang:** Writing – review & editing, Visualization, Supervision, Resources. **Bo Ban:** Writing – review & editing, Supervision, Resources, Funding acquisition. **Dongye He:** Writing – original draft, Validation, Investigation, Funding acquisition, Conceptualization.

Declaration of competing interest

The authors declare that they have no known competing financial interests or personal relationships that could have appeared to influence the work reported in this paper.

Acknowledgements

We are grateful to the patient and her family members for the participation in this study.

Consent to participate

The proband and other family members were recruited from Department of Endocrinology, Genetics and Metabolism at the Affiliated Hospital of Jining Medical University. All participants and/or their legal guardian signed informed consent regarding publishing their data and photographs.

Appendix A. Supplementary data

Supplementary data to this article can be found online at https://doi.org/10.1016/j.heliyon.2024.e28082.

References

[1] J. Herrmann, P.D. Pallister, W. Tiddy, J.M. Opitz, The KBG syndrome-a syndrome of short stature, characteristic facies, mental retardation, macrodontia and skeletal anomalies, Birth Defects Orig, Artic. Ser. 11 (5) (1975) 7–18.
[2] L. Guo, J. Park, E. Yi, E. Marchi, Z.C. Hsieh, Y. Kibalnyk, et al., KBG syndrome: videoconferencing and use of artificial intelligence driven facial phenotyping in 25 new patients, Eur. J. Hum. Genet. 30 (11) (2022) 1244–1254.
[3] A. Sirmaci, M. Spiliopoulos, F. Brancati, E. Powell, D. Duman, A. Abrams, et al., Mutations in ANKRD11 cause KBG syndrome, characterized by intellectual disability, skeletal malformations, and macrodontia, Am. J. Hum. Genet. 89 (2) (2011) 289–294.
[4] E. Martinez-Cayuelas, F. Blanco-Kelly, F. Lopez-Grondona, S.T. Swafiri, R. Lopez-Rodriguez, R. Losada-Del Pozo, et al., Clinical description, molecular delineation and genotype-phenotype correlation in 340 patients with KBG syndrome: addition of 67 new patients, J. Med. Genet. 60 (7) (2023) 644–654.
[5] F.Q. Gao, X. Zhao, B.Y. Cao, X. Fan, X.Q. Li, L.L. Li, et al., Genetic and phenotypic spectrum of KBG syndrome: a report of 13 new Chinese cases and a review of the literature, J. Pers. Med. 12 (3) (2022) 407.
[6] D. Gallagher, A. Voronova, M.A. Zander, G.I. Cancino, A. Bramall, M.P. Krause, et al., Ankrd11 is a chromatin regulator involved in autism that is essential for neural development, Dev. Cell 32 (1) (2015) 31–42.
[7] M.H. Ka, W.Y. Kim, ANKRD11 associated with intellectual disability and autism regulates dendrite differentiation via the BDNF/TrkB signaling pathway, Neurobiol. Dis. 111 (2018) 138–152.
[8] D.M. Roth, P. Baddam, H.M. Lin, M. Vidal-García, J.D. Aponte, S.T. De Souza, et al., The chromatin regulator *Ankrd11* controls palate and cranial bone development, Front. Cell Dev. Biol. 9 (2021) 645836.
[9] Y. Kibalnyk, R. Noble, M. Alexiou, I. Poverennaya, N. Dittmann, A. Greenwell, et al., Ankrd11, a Chromatin Regulator and a KBG Syndrome Risk Gene, Is a Critical Regulator of Cardiac Neural Crest Cell Biology and Heart Development, 2023, https://doi.org/10.21203/rs.3.rs-2605378/v1.

[10] D.Y. He, Y.Y. Li, W.L. Yang, S.X. Chen, H.L. Sun, P. Li, et al., Molecular diagnosis for growth hormone deficiency in Chinese children and adolescents and evaluation of impact of rare genetic variants on treatment efficacy of growth hormone, Clin. Chim. Acta 524 (2022) 1–10.
[11] J.H. Liu, R. Lynn, Chinese sex differences in intelligence: some new evidence, Pers. Indiv. Differ. 75 (2015) 90–93.
[12] K. Low, T. Ashraf, N. Canham, J. Clayton-Smith, C. Deshpande, A. Donaldson, et al., Clinical and genetic aspects of KBG syndrome, Am. J. Med. Genet. 170 (11) (2016) 2835–2846.
[13] I. Parenti, M.B. Mallozzi, I. Hüning, C. Gervasini, A. Kuechler, E. Agolini, et al., ANKRD11 variants: KBG syndrome and beyond, Clin. Genet. 100 (2) (2021) 187–200.
[14] Y. Choi, J. Choi, H. Do, S. Hwang, G.H. Seo, I.H. Choi, et al., KBG syndrome: clinical features and molecular findings in seven unrelated Korean families with a review of the literature, Mol. Genet. Genom. Med. 11 (4) (2023) e2127.
[15] C.F. Wright, D.R. FitzPatrick, H.V. Firth, Paediatric genomics: diagnosing rare disease in children, Nat. Rev. Genet. 19 (5) (2018) 253–268.
[16] R. Kingdom, C.F. Wright, Incomplete penetrance and variable expressivity: from clinical studies to population cohorts, Front. Genet. 13 (2022) 920390.
[17] D.M. Swols, J. Foster, M. Tekin, KBG syndrome, Orphanet J. Rare Dis. 12 (1) (2017) 183.
[18] Q.Y. Li, C.J. Sun, L. Yang, W. Lu, F.H. Luo, Comprehensive analysis of clinical spectrum and genotype associations in Chinese and literature reported KBG syndrome, Transl. Pediatr. 10 (4) (2021) 834–842.
[19] S. Ho, H.M. Luk, I.F.M. Lo, KBG syndrome in a Chinese population: a case series, Am. J. Med. Genet. 188 (6) (2022) 1693–1699.
[20] S. Miyatake, N. Okamoto, Z. Stark, M. Nabetani, Y. Tsurusaki, M. Nakashima, et al., ANKRD11 variants cause variable clinical features associated with KBG syndrome and Coffin-Siris-like syndrome, J. Hum. Genet. 62 (8) (2017) 741–746.
[21] L. Loberti, L.P. Bruno, S. Granata, G. Doddato, S. Resciniti, F. Fava, et al., Natural history of KBG syndrome in a large European cohort, Hum. Mol. Genet. 31 (24) (2022) 4131–4142.
[22] F. Peluso, S.G. Caraffi, G. Contro, L. Valeri, M. Napoli, G. Carboni, et al., Deep phenotyping of the neuroimaging and skeletal features in KBG syndrome: a study of 53 patients and review of the literature, J. Med. Genet. (2023), https://doi.org/10.1136/jmg-2023-109141.
[23] I. Barbaric, M.J. Perry, T.N. Dear, A.R. Da Costa, D. Salopek, A. Marusic, et al., An ENU-induced mutation in the *Ankrd11* gene results in an osteopenia-like phenotype in the mouse mutant Yoda, Physiol. Genomics 32 (3) (2008) 311–321.
[24] R. Libianto, K.H.C. Wu, S. Devery, J.A. Eisman, J.R. Center, KBG syndrome presenting with brachydactyly type E, Bone 123 (2019) 18–22.
[25] O. Kierzkowska, K. Sarino, D. Carter, L.L.Y. Guo, E. Marchi, A. Voronova, et al., Documentation and prevalence of prenatal and neonatal outcomes in a cohort of individuals with KBG syndrome, Am. J. Med. Genet. 191 (9) (2023) 2364–2375.
[26] M.C. Dyle, D. Kolakada, M.A. Cortazar, S. Jagannathan, How to get away with nonsense: mechanisms and consequences of escape from nonsense-mediated RNA decay, Wires. Rna 11 (1) (2020) e1560.
[27] F. Supek, B. Lehner, R.G.H. Lindeboom, To NMD or not to NMD: nonsense-mediated mRNA decay in cancer and other genetic diseases, Trends Genet. 37 (7) (2021) 657–668.
[28] E. de Boer, C.W. Ockeloen, R.A. Kampen, J.E. Hampstead, A.J.M. Dingemans, D. Rots, L. Lütje, et al., Missense variants in ANKRD11 cause KBG syndrome by impairment of stability or transcriptional activity of the encoded protein, Genet. Med. 24 (10) (2022) 2051–2064.
[29] M. Chen, X. Yang, H.Y. Liu, J. Wan, Identification and functional characterization of a bipartite nuclear localization signal in ANKRD11, Biochem. Bioph. Res. Co. 670 (2023) 117–123.
[30] T.T. Zhang, Y. Yang, X.L. Yin, X.Q. Wang, J.H. Ni, Z.Y. Dong, et al., Two loss-of-function ANKRD11 variants in Chinese patients with short stature and a possible molecular pathway, Am. J. Med. Genet. 185 (3) (2021) 710–718.
[31] K. Walz, D. Cohen, P.M. Neilsen, J. Foster, F. Brancati, K. Demir, et al., Characterization of ANKRD11 mutations in humans and mice related to KBG syndrome, Hum. Genet. 134 (2) (2015) 181–190.
[32] N. Borja, M.F. Zafeer, J.A. Rodriguez, D.M. Swols, W. Thorson, G. Bademci, et al., Deletion of first noncoding exon in ANKRD11 leads to KBG syndrome, Am. J. Med. Genet. 191 (4) (2023) 1044–1049.
[33] Z. Awamleh, S. Choufani, C. Cytrynbaum, F.S. Alkuraya, S. Scherer, S. Fernandes, et al., ANKRD11 pathogenic variants and 16q24.3 microdeletions share an altered DNA methylation signature in patients with KBG syndrome, Hum. Mol. Genet. 32 (9) (2023) 1429–1438.